scientific reports

Check for updates

OPEN

Effects of pyrolysis temperatures on the structural properties of straw biochar and its adsorption of tris-(1-chloro-2-propyl) phosphate

Qing Luo✉, Yongyao Deng, Yujie Li, Qing He, Huiqiu Wu & Xu Fang

To investigate the effect of pyrolysis temperature on the adsorption behavior of the emerging organic pollutant tris-(1-chloro-2-propyl) phosphate (TCIPP) on biochar, corn stover was used as raw materials to prepare biochars at different pyrolysis temperatures (250, 350, 500, 700 °C) through limited oxygen carbonization. Elemental analysis, Boehm titration, FTIR, XPS, and other analytical methods were used to reveal the effect of pyrolysis temperature on the physicochemical properties of biochar and its mechanism of TCIPP adsorption. The results showed that the pyrolysis temperature had a significant impact on the physicochemical properties of biochar. As the pyrolysis temperature increases, the specific surface area of biochar rises from 3.083 m^2/g to 435.573 m^2/g, the pH value increases from 6.60 to 10.66, the mass percentage of C increases from 63.10 to 80.58%, and the mass percentage of O decreases from 26.42 to 9.20%. Additionally, the hydrophobicity and aromaticity of biochar also increase with rising pyrolysis temperature, while its polarity decreases. Boehm titration, FTIR, and XPS analysis showed that the total amount of functional groups on the surface of biochar decreased relatively with increasing temperature. Functional groups such as -OH, C=C/C=O, and C-O-C participated in the adsorption of TCIPP on biochar, and ester groups were produced after adsorption. The adsorption process of TCIPP on biochar fits best with the pseudo-second-order equation, indicating that the adsorption process is mainly chemical adsorption, and the main rate-controlling stage is intraparticle diffusion. The isothermal adsorption results were more in line with the Temkin model, indicating that the adsorption process of TCIPP on biochar was mainly surface adsorption. As the pyrolysis temperature increases, the maximum adsorption capacity of biochar increases from 0.8837 mg/g to 2.2574 mg/g. The adsorption process of TCIPP on biochar mainly included pore filling, hydrogen bonding, P-π interaction, hydrophobic interaction, and electrostatic attraction. Among them, pore filling, P-π interaction, and hydrophobic interaction were significantly enhanced with increasing temperature, while hydrogen bonding was relatively weakened. This study will provide a theoretical basis and technical support for the removal of TCIPP from water using biochar adsorption.

Keywords Biochar, Tris-(1-chloro-2-propyl) phosphate, Adsorption mechanism, Pyrolysis temperature, Corn stover

Biochar is a kind of stable, highly aromatic, and carbon-rich porous material prepared by pyrolysis of biomass (crop straws or livestock and poultry manure, etc.) under anaerobic or oxygen-limited conditions, which is usually alkaline under natural conditions[1]. As an organic matter, biochar not only can change the physical and chemical properties of the soil but also has good adsorption capacity due to its large specific surface area and pore structure. It has great potential in carbon sequestration and emission reduction, soil improvement, pollution control, and other aspects, and has gradually become a new type of adsorption material widely used in recent years[2,3].

The adsorption of pollutants by biochar is affected by various factors. Among them, the properties of biochar itself, such as pore size, types of surface functional groups, etc., are the significant factors influencing its adsorption capacity for pollutants[4,5]. Many studies have shown that the preparation temperature can significantly affect the specific surface area, pore structure, surface functional groups, and aromatic structure of biochar, thereby further affecting its adsorption performance for pollutants[6,7]. For example, Zhang et al.[8] found that biochar

Key Laboratory of Eco-restoration of Regional Contaminated Environment, Ministry of Education, Shenyang University, Shenyang 110044, China. ✉email: luoqingyt@126.com

prepared at higher temperatures has a higher degree of aromatization, a larger specific surface area, a more complete pore structure, a decrease in the number of surface polar groups, and a stronger adsorption capacity for simazine. Chen et al.[9] also found that the adsorption performance of orange peel biochar for naphthalene was significantly enhanced with the increase in carbonization temperature.

The physicochemical properties of pollutants are another important factor influencing the adsorption capacity of biochar. Tri(1-chloro-2-propy) phosphate (TCIPP) is a synthetic compound consisting of three chlorinated propyl groups attached to a phosphate ester, which significantly differs in structure and properties from compounds such as polycyclic aromatic hydrocarbons (PAHs) and polychlorinated biphenyls (PCBs). Therefore, even though there are already many studies on the adsorption of organic compounds such as PAHs, PCBs, and petroleum hydrocarbons by biochar[10–12], it is also difficult to directly infer the adsorption behavior of biochar towards TCIPP from these. More importantly, TCIPP, which was listed as a Substance of Very High Concern by the European Union in the fourth batch in 2000[13], has become the primary organophosphate ester (OPE) in various environmental media such as water, soil, and air[14–16]. For example, TCIPP is the most abundant OPE in the water bodies of rivers around the Bohai Rim in China, with concentrations reaching up to 921 ng/L[17]. TCIPP is also the most abundant OPE in the soil in China, accounting for 39.6% of total OPEs and reaching concentrations of up to 401 μg/kg[16]. Additionally, TCIPP is the dominant OPE in sediments from the artificial Shiwa Lake in South Korea, with concentrations reaching 2500 μg/kg[18]. Hence, to effectively prevent and control TCIPP pollution in the environment, it is highly necessary to research the adsorption behavior of biochar towards TCIPP.

Our previous research found that corn straw biochar has good adsorption capacity for TCIPP, and its adsorption is influenced by multiple processes and factors. However, there is still a lack of in-depth exploration of the specific adsorption mechanism, and there are few reports on the impact of pyrolysis temperature on the performance and mechanism of biochar adsorption of TCIPP[19]. Therefore, this study continues to use corn straw as the raw material to prepare biochar at different pyrolysis temperatures (250, 350, 500, 700 ℃). We aim to explore the influence of preparation temperature on the structural properties of corn straw biochar and its adsorption capacity for TCIPP, investigate the correlation between the physicochemical properties of biochar and its adsorption performance, and attempt to reveal the adsorption mechanism of biochar for TCIPP. This study aims to provide theoretical support for the application of biochar in the remediation of organic-polluted water.

Materials and methods

Preparation of biochar

The corn stover employed in the study originated from Chaoyang City, Liaoning Province, China. Before utilization, it underwent a rigorous process that included washing, air-drying, and further drying in an oven at 75 °C. After pulverization, the stover was poured into a crucible and underwent pyrolysis for 6 h in a muffle furnace (Jinan Precision Scientific Instrument Co., Ltd., SX2-12-10, China) under oxygen-limited conditions at various temperatures (250, 350, 500, and 700 °C). To achieve slow pyrolysis, the heating rate of the muffle furnace was set at 5 °C/min. Once cooled to room temperature, it was ground and sieved through a 100-mesh sieve, resulting in four distinct samples labeled as CS250, CS350, CS500, and CS700.

Characterization of biochar

The surface morphology of biochar was observed and analyzed using a scanning electron microscope (S4800, Japan). The elemental composition (C, H, N) was determined by an elemental analyzer (Elementar-Vario EL cube, Germany). The ash content was calculated as the remaining sample mass after biochar was burned at 800 °C for 4 h, and the O element content was obtained by mass difference subtraction. The specific surface area and pore volume were measured using a specific surface area and pore size analyzer (JW-BK122F static nitrogen adsorption instrument, Beijing). The content of surface functional groups on biochar was quantitatively determined and analyzed using the Boehm titration method[20]. In brief, the solutions of $NaHCO_3$, Na_2CO_3, NaOH, and C_2H_5ONa were mixed with biochar respectively, shaken, followed by filtration. The filtrate was then titrated with a standardized HCl solution to the endpoint. By utilizing the differences in the amounts of neutralizing reagents used for the four types of solutions, the contents of various oxygen-containing functional groups can be determined. The crystal structure on the surface of biochar was characterized using an X-ray polycrystalline diffractometer (UltimaIV, Japan). The changes in surface functional groups of biochar before and after adsorption were analyzed using a Fourier Transform Infrared Spectrometer (IRTracer 100, Japan). The changes in the main elements and chemical states on the surface of biochar before and after adsorption were characterized using an X-ray Photoelectron Spectrometer (Thermo Scientific Escalab 250Xi, USA). The pH value is represented by the pH of the solution measured after mixing biochar with deionized water in a ratio of 1 to 20 (g: mL).

Adsorption experiment

Adsorption dynamics experiment

Separately weigh 4 mg of different biochar samples and add them to a TCIPP solution with a mass concentration of 500 μg/L, maintaining a solid-liquid ratio of 1:2. Place the mixtures in a shaker maintained at a constant temperature of 25 °C and shake them at a speed of 120 r/min. Collect samples at 0, 5, 15, 30, 60, 90, 120, 240, 300, 480, 600, and 1080 min. After filtering the samples through a 0.22 μm organic nylon filter membrane, directly measure the TCIPP concentration in the solution using UPLC-MS/MS. Repeat each experiment three times.

A blank control experiment was also conducted, which solely consisted of TCIPP without the addition of biochar. Upon achieving adsorption equilibrium, the average recovery rate of TCIPP was found to be 94.89%.

This result suggests that the influence of experimental materials and the volatilization of TCIPP during the adsorption process were insignificant.

Isothermal adsorption experiment
Separately weigh 4 mg of different biochar samples and add them to TCIPP solutions with mass concentrations of 50, 100, 200, 300, 400, 600, 800, and 1000 μg/L, maintaining a solid-liquid ratio of 1:2. Place the mixtures in a shaker maintained at a constant temperature of 25 °C and shake them at a speed of 120 r/min until equilibrium is attained. After filtering the mixtures through a 0.22 μm organic nylon filter membrane, directly measure the TCIPP concentration in the solution using UPLC-MS/MS. Repeat each experiment three times.

Determination of TCIPP

The concentration of TCIPP in the solution was determined using UPLC-MS/MS (Ultimate 3000/TSQ Endura, Thermo Scientific). A Thermo Hypersil GOLD column (2.1 mm × 100 mm, 3 μm) was used, with a mobile phase consisting of methanol and ultrapure water (V: V = 70: 30). The flow rate of the mobile phase was set at 0.3 mL/min, the column temperature was 40 °C, and the injection volume was 5 μL. Electrospray ionization (ESI) source was employed in positive ion mode, with a peak width resolution of 0.7 m/z. The spray voltage was set at 3500 V, the ion transfer tube temperature was 350 °C, and the collision gas pressure was 2 mTorr. Quantitative analysis was performed using a multiple reaction monitoring (MRM) mode. Detailed parameters can be found in the literature by Luo et al.[21].

Data processing and analysis

The calculation of the adsorption capacity (Q_e) of biochar for TCIPP is as follows:

$$Q_e = \frac{(C_0 - C_e)\,V}{m} \tag{1}$$

Where, Q_e is the adsorption capacity at equilibrium, mg/g; C_0 and C_e are the initial concentration and equilibrium concentration of the TCIPP solution, respectively, mg/L; V is the volume of the TCIPP solution, L; m is the mass of the biochar, mg.

The adsorption kinetic experimental data were fitted and analyzed using pseudo-first-order, and pseudo-second-order kinetic equations, and intra-particle diffusion equations. The fitting equations are as follows:

$$\text{Pseudo}-\text{first}-\text{order kinetic}: \; Q_t = Q_e\left(1 - e^{k_1 t}\right) \tag{2}$$

$$\text{Pseudo}-\text{second}-\text{order kinetic}: \; Q_t = \frac{k_2 Q_e^2 t}{1 + k_2 Q_e t} \tag{3}$$

$$\text{Intra}-\text{particle diffusion}: \; Q_t = k_i t^{0.5} + C \tag{4}$$

Where, Q_t stands for the adsorption capacity at time t, mg/g; k_1 and k_2 represent the adsorption rate constants of pseudo-first-order and pseudo-second-order kinetics, the units are 1/h and g/mg/h, respectively; k_i is the intraparticle diffusion rate constant, mg/(g·min$^{0.5}$); C is a constant related to the thickness of the boundary layer.

The isothermal adsorption experiment data were fitted and analyzed using Langmuir, Freundlich, and Temkin models. The fitting equations are as follows:

$$Langmuir: \; Q_e = \frac{Q_{max} k_L C_e}{1 + k_L C_e} \tag{5}$$

$$\text{Freundlich}: Q_e = k_F C_e^{\frac{1}{n}} \tag{6}$$

$$\text{Temkin} = Q_e = a \ln(k_T) + a \ln(C_e) \tag{7}$$

Where, Q_{max} represents the maximum adsorption capacity when adsorption equilibrium is reached, mg/g; K_L is the adsorption constant of the Langmuir equation, L/g; K_F is the adsorption constant of the Freundlich equation, (mg/g)·(L/g)$^{1/n}$; n is the equilibrium parameter of the Freundlich equation; K_T is a constant related to the bond energy; a refers to Kelvin temperature.

Statistical analysis and processing of experimental data were conducted using Excel. Phase analysis of XRD data was performed using Jade 6 software. XPS data results of biochar were processed, peak-fitted, and analyzed using XPS PEAK 4.1 software. FTIR data was processed and analyzed using OMNIC software. SPSS 26 software was used to perform a significant difference analysis on the adsorption experimental results. Equation fitting of the adsorption experimental data was done with Origin 9.0 Pro. All graphs in the document were created using Origin software.

Results and discussion

Properties of biochar

Surface morphology
The scanning electron microscopy (SEM) analysis of biochar (Fig. 1) shows that there are significant differences in the surface morphology of biochar at different preparation temperatures. When the pyrolysis temperature is relatively low, the surface of the biochar is smoother and the structure is compact, with fewer pore distributions. This may be due to the low temperature, resulting in incomplete carbonization of the biomass. As the

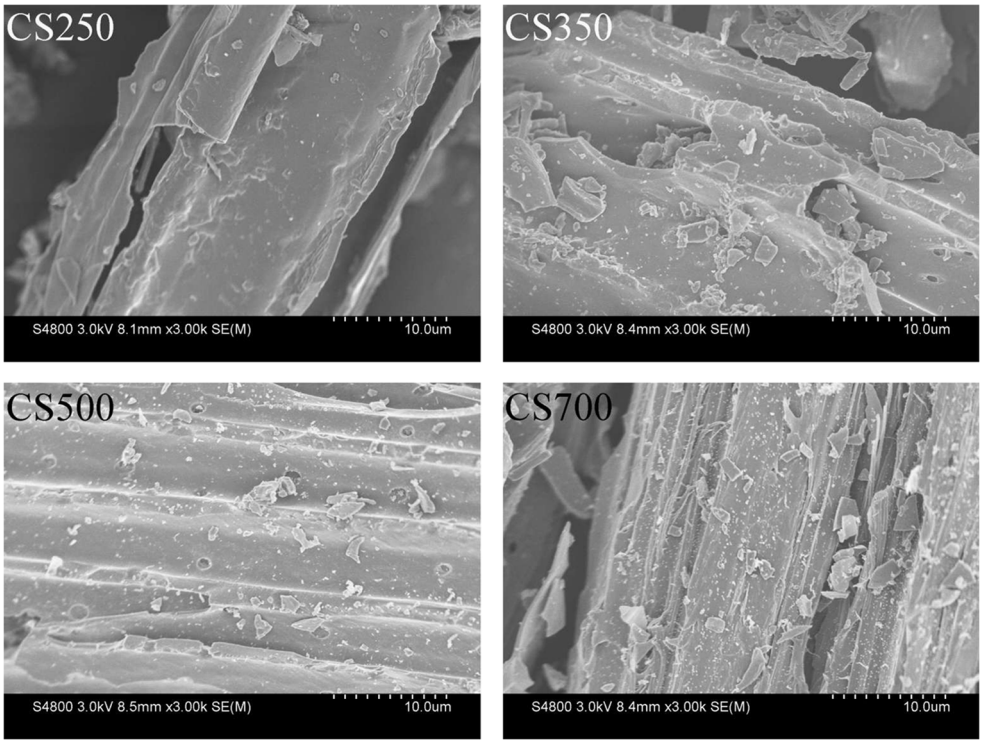

Fig. 1. SEM images of biochar (×3000).

Biochar		CS250	CS350	CS500	CS700
Element mass percentage	C (%)	63.10	68.63	78.63	80.58
	H (%)	1.63	1.54	1.36	1.21
	N (%)	4.59	4.30	1.97	1.35
	O (%)	26.42	20.26	11.70	9.20
Atomic ratio	H/C	0.073	0.063	0.025	0.017
	O/C	0.419	0.295	0.149	0.114
	(O + N)/C	0.444	0.318	0.166	0.129
Ash (%)		4.27	5.27	6.35	7.67
pH		6.60	7.55	10.00	10.66
BET ($m^{2/g}$)		3.083	14.284	215.937	435.573
Total pore volume (cm^3/g)		0.011	0.020	0.135	0.258
Average pore diameter (nm)		13.838	5.688	2.492	2.368

Table 1. Physicochemical properties of biochar.

temperature increases, a large number of distinct and irregularly shaped pores begin to form on the surface of the biochar. This is caused by the volatile substances produced by the decomposition of lignocellulose in the biochar escaping. When the temperature rises to 700 ℃, the microstructure of the biochar is destroyed, the surface roughness increases and a large number of particulate and blocky fragments appear. This may be due to the gradual decomposition of the biomass at excessively high temperatures, leading to a large amount of ash accumulating on the surface[22].

Elemental composition and specific surface area

The basic physicochemical properties of straw biochar prepared at different carbonization temperatures are shown in Table 1. As the temperature increases, the ash content in the biochar increases from 4.27 to 7.67%, and the C element content increases from 63.10 to 80.58%. Meanwhile, the H and O element contents decrease from 1.63% and 26.42–1.21% and 9.20%, respectively, indicating that dehydrogenation and deoxidation reactions occur during straw pyrolysis, and the carbonization degree of biochar increases significantly[23]. The (O + N)/C, O/C, and H/C ratios of biochar can reflect the polarity, hydrophilicity, and aromaticity of biochar, respectively. Higher (O + N)/C and O/C ratios indicate higher hydrophilicity and polarity of biochar, while a lower H/C ratio indicates a higher degree of aromatization of biochar[24]. As can be seen from Table 1, the O/C, H/C, and (O + N)/C

ratios of biochar gradually decrease, indicating that as the biochar temperature increases, the aromaticity and hydrophobicity of biochar increase, and the polarity index decreases.

The specific surface area and total pore volume of biochar increase significantly with increasing temperature, while the average pore diameter decreases significantly. This is because when the carbonization temperature is low, organic components such as hemicellulose, lignin, and cellulose in the biochar are not completely decomposed, resulting in fewer pores formed on the surface of the biochar. However, at higher temperatures, a large amount of organic matter in the biomass is decomposed into volatile substances or gases that escape, generating a large number of pore structures[8]. In addition, the pH value of biochar gradually increases with increasing temperature, which may be due to the gradual volatilization and reduction of a large amount of acidic substances in the biochar as the temperature gradually increases, as well as the gradual melting and formation of alkaline substances from weak acid salts in the biochar under high-temperature conditions[25].

Crystal structure

X-ray diffraction (XRD) can directly analyze the mineral components contained in biochar. Figure 2 shows the XRD patterns of biochar prepared at different temperatures. As can be seen from the figure, corn stalk biochar is rich in KCl components. As the temperature increases, the KCl diffraction peaks at $2\theta = 28.35°$ and 40.52° become more intense, and new diffraction peaks appear at $2\theta = 50.19°$ and 66.40°. When the carbonization temperature rises to 500 ℃, diffraction peaks of $CaCO_3$ and SiO_2 crystals begin to appear at $2\theta = 29.48°$ and 74.02°, respectively. This may be because as the temperature of the biochar increases, the biomass gradually decomposes completely, leading to an increase in the ash content of the biochar and an increase in the crystallinity of the biochar[26,27].

Surface functional group content

The quantitative changes in the number of surface functional groups of biochar can be measured by Boehm titration. Table 2 shows the quantitative changes in the number of surface functional groups of biochar at different pyrolysis temperatures. As can be seen from the table, the total amount of basic functional groups on the surface of biochar at different temperatures is significantly lower than that of acidic functional groups, and as the temperature increases, the number of basic functional groups on the surface of biochar gradually increases, from 0.08 mmol/g to 0.17 mmol/g; while the number of acidic groups decreases significantly, from 1.04 mmol/g to 0.49 mmol/g, which is consistent with the change law of pH value of biochar. In addition, the number of lactone groups (-COOR), phenolic hydroxyl groups (-OH), and carboxyl groups (-COOH) on the surface of biochar gradually decreases as the temperature of biochar increases, while the number of carbonyl groups (-C=O) gradually increases, but the total amount of acidic oxygen-containing functional groups shows a decreasing trend, which is consistent with the FTIR analysis results of biochar.

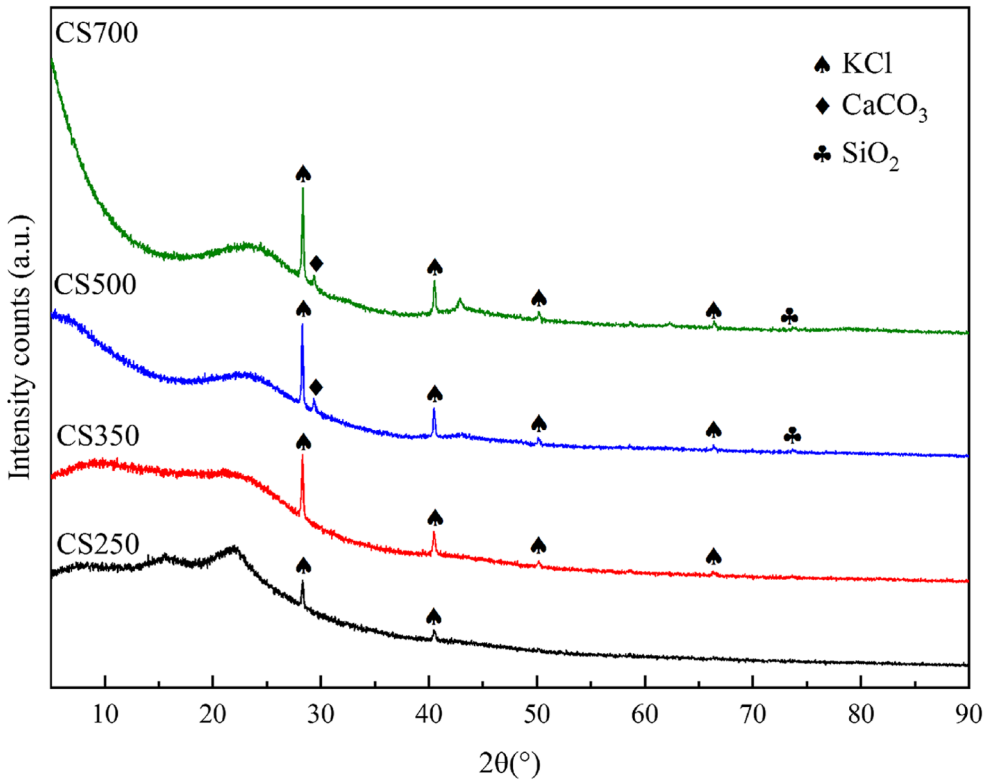

Fig. 2. XRD spectra of biochar.

Biochar	Basic functional groups (mmol/g)	Acidic functional groups (mmol/g)				Oxygen-containing functional group (mmol/g)
		-COOR	-C=O	-COOH	-OH	
CS250	0.08	0.32	0.08	0.50	0.14	1.04
CS350	0.11	0.22	0.10	0.41	0.29	1.02
CS500	0.15	0.11	0.16	0.21	0.17	0.65
CS700	0.17	0.06	0.24	0.08	0.11	0.49

Table 2. Surface functional group content of biochar.

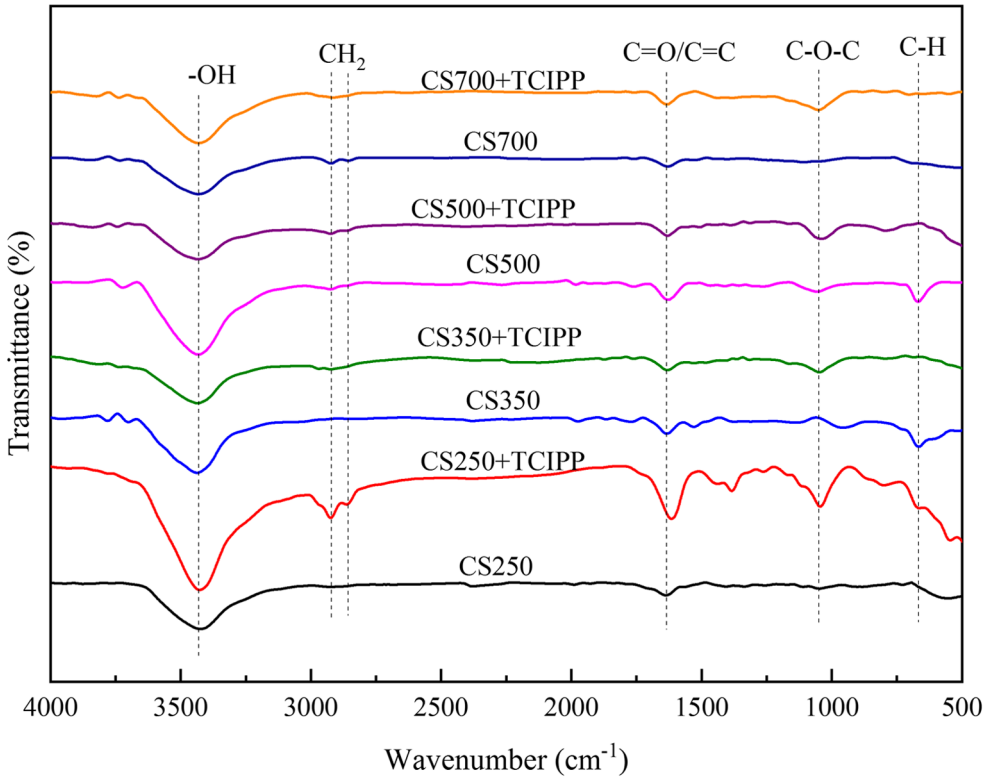

Fig. 3. FTIR spectra of biochar before and after adsorption.

FTIR

As can be seen from the FTIR spectrum of biochar (Fig. 3), there are significant differences in the content of surface functional groups of biochar at different pyrolysis temperatures. As the biochar temperature increases, the stretching vibration peak of -OH at a wavelength of 3432 cm^{-1} gradually weakens, which may be due to the detachment of bound water during pyrolysis, leading to the breaking of hydroxyl groups bound by hydrogen bonds[28]. The stretching vibration peaks of aliphatic CH2 around 2924 cm^{-1} and 2855 cm^{-1} show no significant change in peak intensity with increasing temperature. The peak near 1632 cm^{-1} corresponds to the stretching vibration peak of C=C/C=O, and the peak intensity is relatively stable. However, the vibration peak of C-O-C at 1052 cm^{-1} significantly increases with increasing carbonization temperature, which may be due to the decomposition of organic components such as cellulose and lignin in straw biochar as the temperature increases, resulting in the gradual breaking of bonds in the aromatic ring structure and the formation of volatile substances that gradually decrease[9]. In addition, the deformation absorption peak of C-H on the aromatic ring at 669 cm^{-1} increases with increasing temperature, indicating that aromatic structures are formed during the pyrolysis of biochar and the degree of aromatization increases, consistent with the elemental analysis results[29].

XPS

The XPS full spectrum of biochar is shown in Fig. 4. As can be seen from the figure, the main elements on the surface of biochar are C and O, with C1s peak at 284.8 eV and O1s peak at 533.1 eV. As the preparation temperature increases, the spectral peak intensity of C1s in the functional groups on the surface of biochar is significantly enhanced (from 79.42 to 91.02%), while the spectral peak intensity of O1s is significantly reduced (from 20.58 to 8.98%), indicating that the biochar is gradually decomposed completely with the increase of temperature. The peak fitting of C1s and O1s characteristic peaks of biochar was carried out separately. The C1s

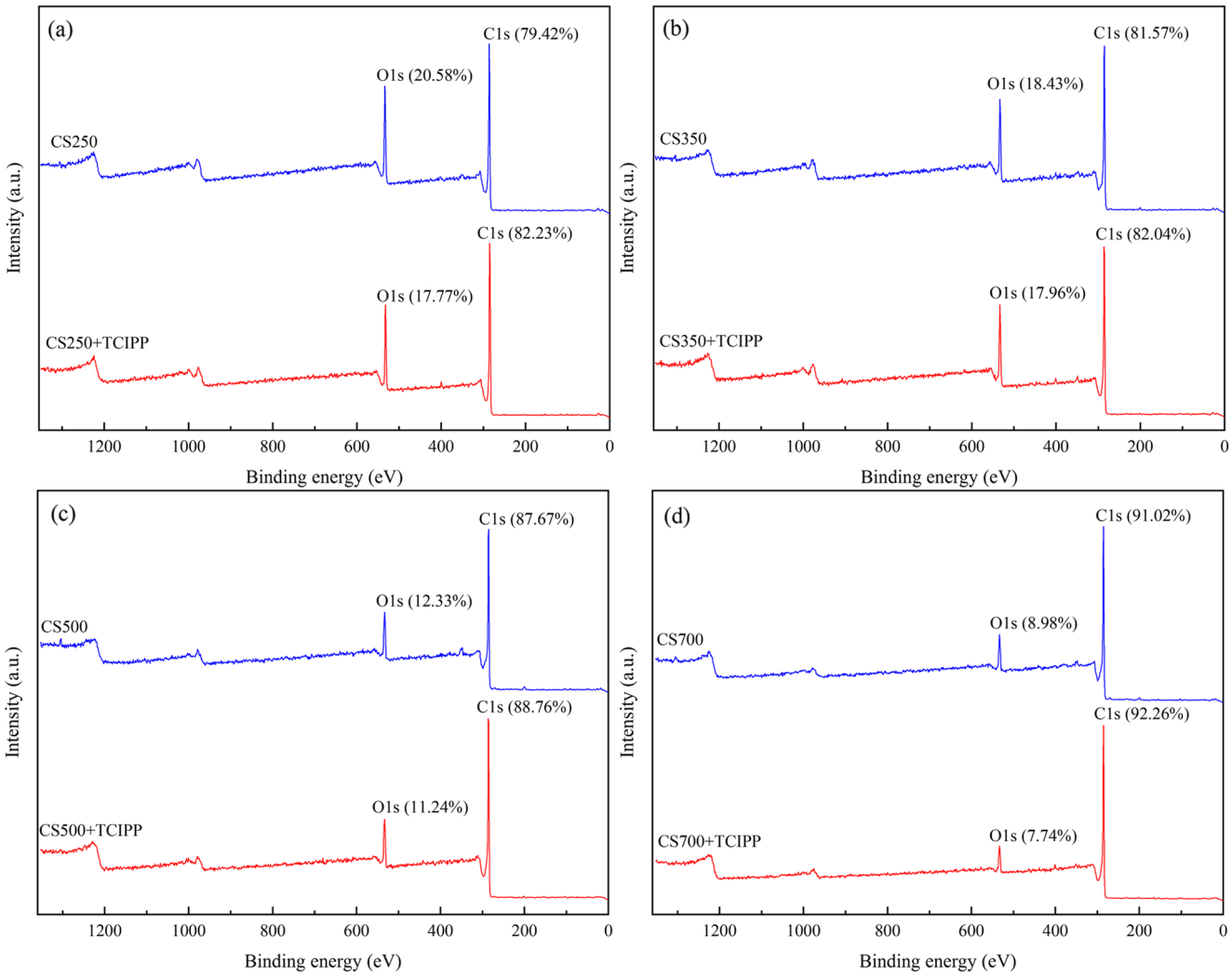

Fig. 4. XPS of biochar before and after adsorption.

Line	Binding energy/eV	Chemical Bonds / Functional Groups	Atomic percentage/%							
			CS250	CS250 + T	CS350	CS350 + T	CS500	CS500 + T	CS700	CS700 + T
C1s	284.8	C-C	69.82	68.60	70.08	63.39	73.41	69.63	75.25	75.17
	285.7	C-O	15.93	13.49	14.83	13.53	13.35	12.84	13.20	11.56
	287.0	C=O	9.60	12.27	9.21	17.71	8.10	11.83	6.16	7.63
	288.9	O=C-O	4.55	5.64	5.07	5.37	5.14	5.70	5.39	5.64
O1s	531.5	C=O	23.52	25.46	25.68	29.87	28.04	28.88	30.79	32.28
	532.3	O-H	34.51	36.49	35.55	33.32	34.29	34.97	34.30	33.70
	533.2	C-O-C	23.06	24.28	23.43	23.25	21.02	22.97	20.74	21.96
	534.2	C-OOH	15.91	13.77	15.34	13.56	14.65	13.18	14.17	12.06

Table 3. C1s and O1s binding states and relative atomic percentages on the biochar surfaces.

and O1s spectra after peak separation were composed of 4 parts, and the results are shown in Fig. S1 and S2. As can be seen from the figures, most of the carbon atoms on the surface of straw biochar exist in the form of C-C, with a small part combining with oxygen; while most of the oxygen atoms exist in the form of O-H. According to the changes in the binding energy, chemical bonds, and atomic percentages of carbon and oxygen atoms on the surface of biochar (Table 3), the proportion of C-C and O=C-O on the surface of biochar increases with the increase of temperature, while the proportion of O-H, C-O-C, and C-OOH functional groups decreases significantly, indicating that the total amount of oxygen-containing functional groups on the surface of biochar

decreases with the increase of temperature, and the aromaticity of biochar increases[30,31], which is consistent with the results of Boehm functional group titration and FTIR analysis.

Adsorption experiments

Adsorption kinetics

The curve showing the variation of TCIPP adsorption capacity by biochar at different pyrolysis temperatures to adsorption time is presented in Fig. 5a. As can be seen from the figure, the adsorption capacity of biochar for TCIPP increases rapidly within the first 4 h, during which time there are many adsorption sites on the surface of the biochar, allowing for rapid adsorption of TCIPP from the solution. Afterward, the curve gradually becomes smoother as the adsorption sites on the biochar surface become gradually saturated. At the same time, the electrostatic repulsion between the biochar and TCIPP increases, leading to the adsorption reaching an equilibrium state.

The results of biochar adsorption of TCIPP were analyzed and fitted using pseudo-first-order, pseudo-second-order, and intraparticle diffusion equations, as shown in Fig. 5b, c, d and Table 4. The R^2 value of the pseudo-second-order kinetic model fit is significantly higher than that of the pseudo-first-order kinetic model, and the maximum adsorption capacity (Q_e) calculated by the pseudo-second-order equation is closer to the actual maximum adsorption capacity, indicating that the pseudo-second-order kinetic model can more reasonably explain the adsorption process of TCIPP by biochar. Some studies have indicated that adsorption conforming to the pseudo-second-order kinetic model is primarily chemical adsorption[32]. Therefore, the adsorption of TCIPP by biochar in this study is a chemical adsorption process. The straight line of the intraparticle diffusion equation does not pass through the origin, indicating that the adsorption of TCIPP on biochar is not solely controlled by the intraparticle diffusion process. The entire adsorption process follows three stages: intraparticle diffusion stage, surface adsorption stage, and liquid film diffusion stage. In addition, the value of K_i can be used to indicate the ease of dispersion of TCIPP within the biochar, and a larger value of K_i indicates that the diffusion of TCIPP within the biochar is more likely to occur. The parameters of the intraparticle diffusion stages are $K_1 > K_2 > K_3$, indicating that the diffusion rates of each stage during the entire adsorption process are: liquid film diffusion

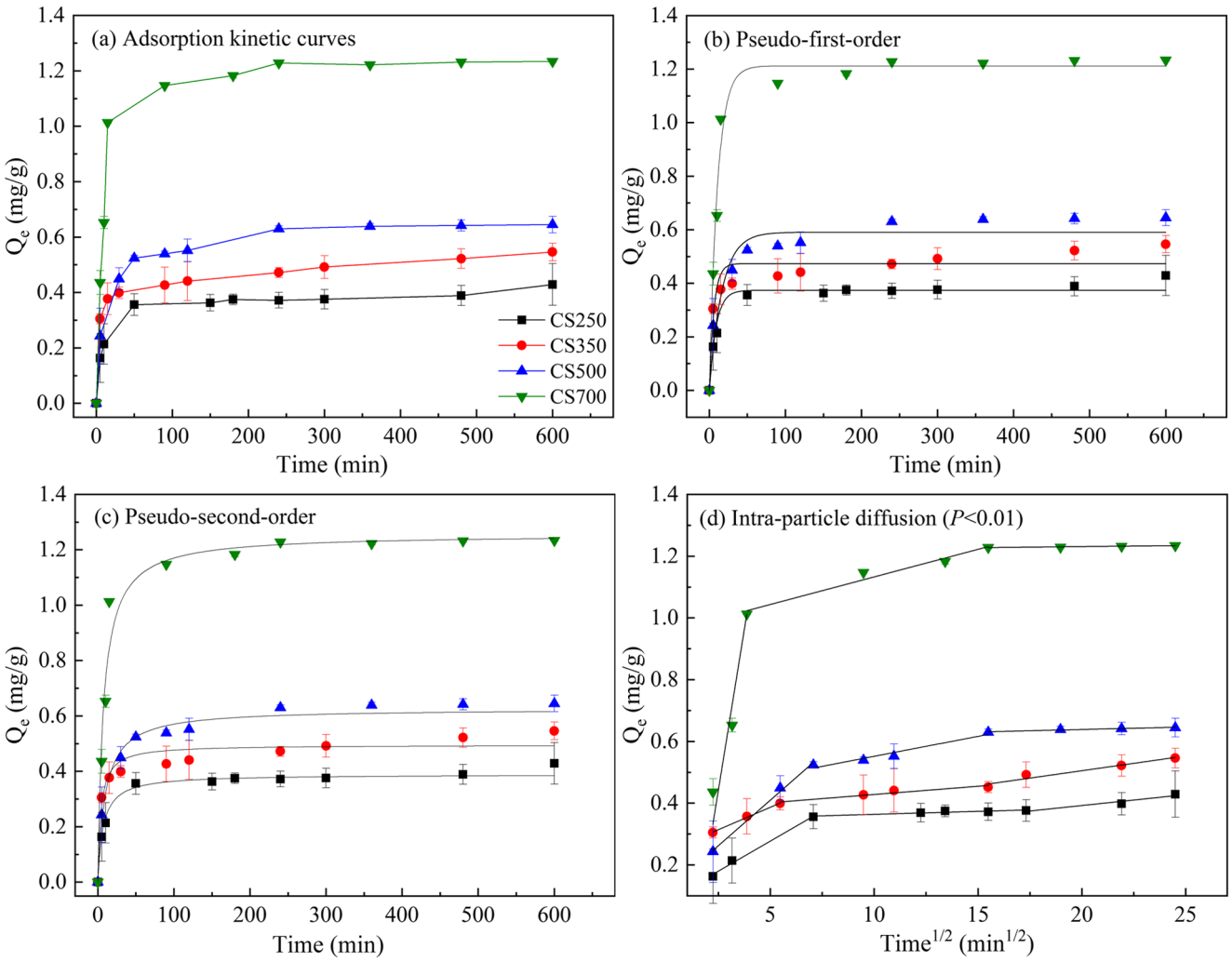

Fig. 5. Adsorption dynamics fitting curves of biochar for TCIPP.

Biochar	Pseudo-first-order			Pseudo-second-order			Intra-particle diffusion								
							I			II			III		
	K_1	Q_e	R^2	K_2	Q_e	R^2	K_1	C_1	R^2	K_2	C_2	R^2	K_3	C_3	R^2
CS250	0.1429	0.3746	0.9406	0.5705	0.3858	0.9511	0.0389	0.0828	0.9884	0.0071	0.3443	0.817	0.0019	0.2505	80.8703
CS350	0.1649	0.4732	0.9011	0.5072	0.4951	0.9535	0.029	0.2416	0.9939	0.0096	0.3746	0.8882	0.0053	0.3139	0.9202
CS500	0.0601	0.5903	0.9407	0.1646	0.6256	0.9876	0.0589	0.115	0.9906	0.013	0.4216	0.9243	0.0016	0.6061	0.9191
CS700	0.0933	1.2114	0.9728	0.1090	1.2552	0.9842	0.3467	0.3706	0.9066	0.0179	0.9541	0.9546	0.0007	1.2168	0.924

Table 4. Fitting parameters for the adsorption kinetics of biochar for TCIPP.

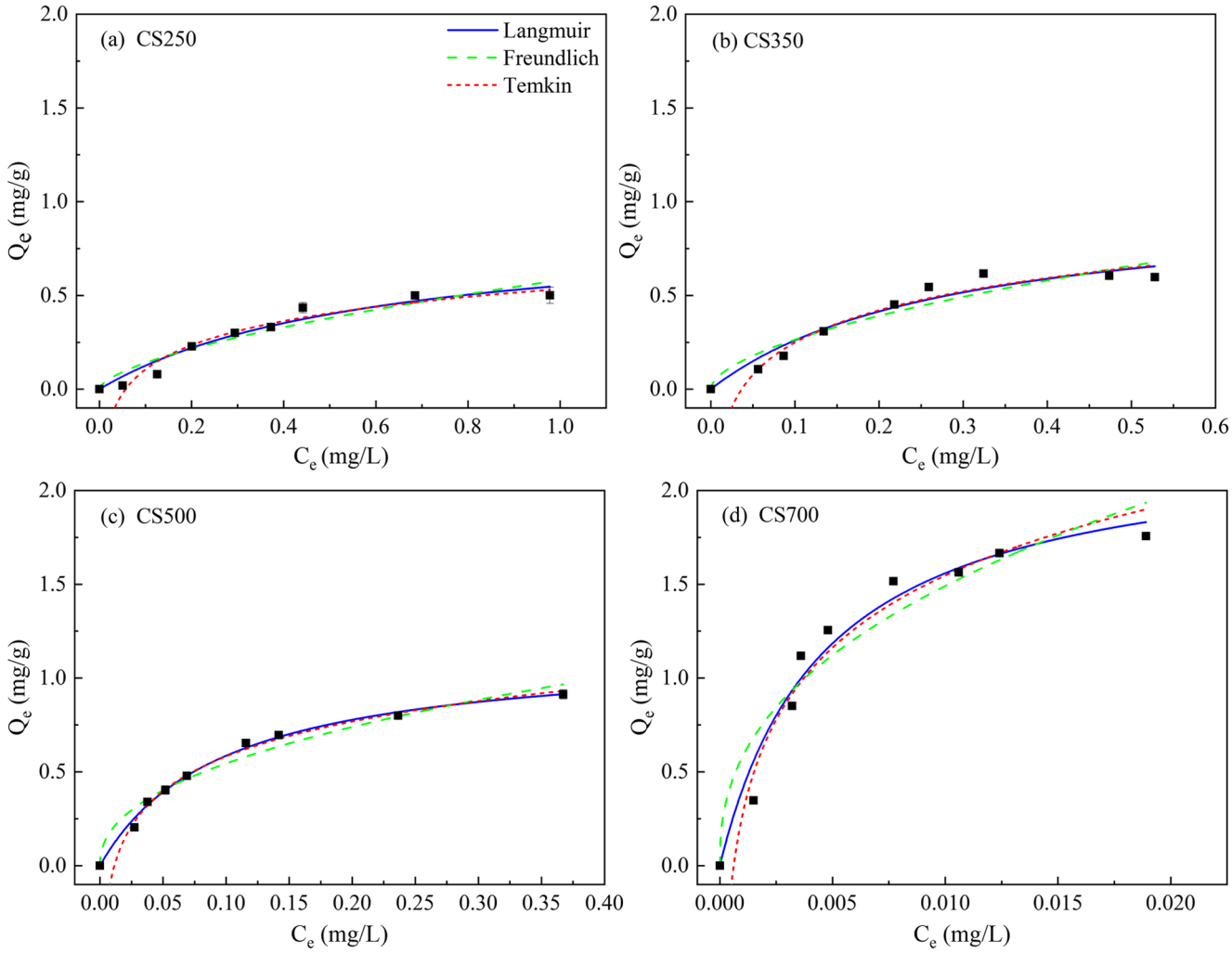

Fig. 6. Adsorption isothermal fitting curve of biochars for TCIPP.

Biochar	Langmuir			Freundlich			Temkin		
	k_L	q_m	R^2	k_F	n	R^2	k_T	a	R^2
CS250	1.6576	0.8837	0.9463	0.5815	1.6222	0.9009	17.6054	0.1863	0.9570
CS350	3.54534	1.0147	0.9452	0.9741	1.7657	0.9003	27.3137	0.2479	0.9600
CS500	10.2601	1.1567	0.9938	1.5025	2.2707	0.9623	87.7384	0.2683	0.9948
CS700	220.9934	2.2574	0.9650	9.6706	2.4597	0.9129	1622.9043	0.5551	0.9661

Table 5. Fitting parameters for isothermal adsorption of biochar for TCIPP. ($P < 0.01$).

rate > surface adsorption rate > intraparticle diffusion rate, with the intraparticle diffusion stage being the main rate-controlling process[33]. In addition, the non-zero value of C also indicates that the entire adsorption process is affected by multiple stages[34].

Adsorption isotherm

As shown in Fig. 6, as the initial concentration of TCIPP increases, the adsorption capacity of biochar for TCIPP increases significantly ($P < 0.01$) and then gradually reaches equilibrium. This is mainly because when the concentration of TCIPP is low, biochar can provide more adsorption sites for the adsorption process of TCIPP, which is conducive to the rapid adsorption of TCIPP by biochar. However, as the concentration of TCIPP continues to increase, the rate of increase in adsorption capacity slows down, which may be due to the gradual saturation of active sites on the surface of biochar[35].

As shown in Table 5, the R^2 values of the fitting results of the three models for the adsorption process are all high, but the adsorption of TCIPP by biochar is most consistent with the Temkin model, indicating that the adsorption process is dominated by irregular surface adsorption with the coexistence of electrostatic

interactions[36]. In addition, the maximum adsorption capacity of biochar for TCIPP increases significantly with the increase in temperature, and the order of adsorption capacity is CS700 (2.2574 mg/g) > CS500 (1.1567 mg/g) > CS350 (1.0147 mg/g) > CS250 (0.8837 mg/g). The n and K_F values in the Freundlich model can reflect the adsorption capacity of biochar[37]. The smaller the value of $1/n$, the better the adsorption effect of biochar. The $1/n$ values (0.4066–0.6164) of straw biochar for TCIPP adsorption are all less than 1, indicating that the adsorption process of biochar for TCIPP is easy to occur. As the temperature increases, the K_F value also gradually increases, indicating that the adsorption performance of biochar for TCIPP gradually improves with the increase in temperature.

Effect of physicochemical properties of biochar

The pore structure and physicochemical properties of biochar play an important role in its adsorption process of various organic pollutants[24]. The correlations between the relevant parameters (Q, K_F, and n values) of the Langmuir and Freundlich equations for biochar adsorption of TCIPP and the polarity index, aromaticity, and hydrophilicity [(O + N)/C, H/C, O/C] of the biochar are shown in Fig. 7. As can be seen from the figure, there is a good positive correlation between the specific surface area (SA) of biochar and its adsorption capacity (Q) for TCIPP, indicating that the adsorption capacity of biochar for TCIPP increases significantly with the increase of specific surface area ($P < 0.01$). The K_F and n values of the Freundlich equation have a good negative correlation with the polarity index, aromaticity, and hydrophilicity [(O + N)/C, H/C, O/C] of the biochar. As the temperature increases, the hydrophobicity and aromaticity of biochar increase significantly, while the polarity decreases, and the adsorption capacity of biochar for TCIPP increases, indicating that there may be hydrophobic interactions between biochar and the hydrophobic organic pollutant TCIPP. Ahmad et al.[38] pointed out that the relationship between K_F and n values and polarity index, aromaticity, and hydrophilicity [(O + N)/C, H/C, O/C], can be used to indicate the role of components in biochar during the adsorption process. In this study, they exhibited a linear relationship, suggesting that the organic components in biochar play a significant role in the adsorption process of TCIPP.

Adsorption mechanism

The adsorption of biochar to organic pollutants mainly includes the partition effect and surface adsorption. According to the isothermal adsorption results of biochar to TCIPP, the adsorption process of TCIPP on the surface of biochar is mainly surface adsorption, with electrostatic interaction involved. The acidic functional groups (such as carboxyl, ester, hydroxyl, etc.) on the surface of biochar are prone to undergo surface adsorption with polar compounds through chemical bonding forces[39,40]. And since TCIPP belongs to a compound with relatively strong polarity, this also indicates the presence of surface adsorption.

Research shows that the surface adsorption of biochar to organic pollutants includes physical adsorption (hydrophobic interaction, van der Waals force, electrostatic attraction) and chemical adsorption (hydrogen bonding, etc.)[9]. In this study, as the carbonization temperature increases, the hydrophobicity of biochar gradually increases, and its adsorption capacity for TCIPP also gradually increases, indicating that the hydrophobic interaction between biochar and TCIPP is significantly enhanced. The good positive correlation between the specific surface area of biochar and the adsorption amount also indicates that pore filling may be one of the

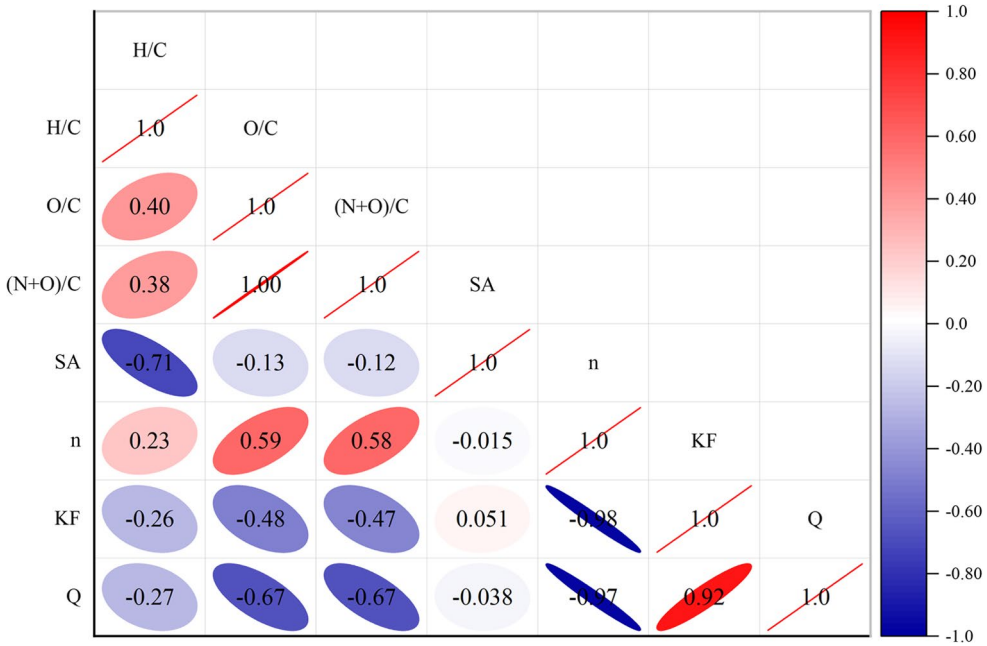

Fig. 7. Heat map of correlation between parameters related to isothermal adsorption equation and physicochemical properties of biochar.

factors affecting the adsorption effect of TCIPP on biochar. With the increase in temperature, the specific surface area and total pore volume of biochar significantly increase, and the pore-filling effect of biochar on TCIPP is significantly enhanced.

Compared to before adsorption, the content of surface functional groups of biochar after TCIPP adsorption undergoes significant changes (Fig. 3). The characteristic peak of -OH relatively weakens, indicating that hydrogen bonding occurs during the adsorption of TCIPP by biochar. The C=C/C=O on the aromatic ring significantly increases, which may be due to the formation of a more stable structure through P-π interactions between the P in TCIPP and the aromatic hydrocarbon ring on the biochar surface[41]. In addition, the significant increase in the vibration peak of C-O-C after adsorption indicates that ester groups are produced on the biochar after TCIPP adsorption.

After biochar adsorbs TCIPP (Fig. 4), the content of C element in the surface functional groups increases relatively, while the content of O element decreases significantly, indicating that the oxygen-containing groups on the surface of biochar participate in the process of adsorbing TCIPP. Further peak fitting revealed that the content of C-O-C and O=C-O on the surface of biochar increased relatively after adsorption of TCIPP, while the content of C-OOH and O-H decreased relatively (Fig.S1 and S2, Table 3), indicating that esters and carbonyl groups were generated on the surface of biochar after adsorption of TCIPP, and hydrogen bonding may occur between O-H on the surface of biochar and TCIPP[31,42], which is consistent with the FTIR analysis results of biochar before and after adsorption.

FTIR and XPS analysis before and after biochar adsorption of TCIPP showed that hydrogen bonding and P-π interaction were involved in the adsorption process of biochar to TCIPP, and as the temperature of biochar increased, the hydrogen bonding effect of biochar on TCIPP decreased significantly, while the P-π interaction increased continuously. In summary, the adsorption mechanism of biochar to TCIPP mainly includes pore filling, hydrogen bonding, P-π interaction, hydrophobic interaction, and electrostatic attraction. As the temperature increases, the adsorption effect of biochar on TCIPP significantly improves, among which pore filling, P-π interaction, and hydrophobic effect are significantly enhanced, while hydrogen bonding is weakened.

Conclusions

This study prepared straw biochar under the conditions of 250, 350, 500, and 700 °C, and explored the influence of pyrolysis temperature on the physicochemical properties of biochar and its adsorption of TCIPP. Pyrolysis temperature is one of the important factors affecting the physical and chemical properties of biochar. As the temperature increases, the content of hydrogen and nitrogen elements in straw biochar gradually decreases, while the content of carbon elements significantly increases. The polarity of biochar decreases, hydrophobicity and aromaticity increase, and the ash content, pH value, total pore volume, and specific surface area of biochar all increase significantly. The main component of biochar is KCl, and the diffraction peak of KCl crystals gradually increases as the temperature rises. The total amount of functional groups on the surface of biochar decreases relatively with increasing temperature. Functional groups such as -OH, C=C/C=O, and C-O-C participate in the adsorption of TCIPP on biochar, and ester groups are produced after adsorption. Adsorption kinetics indicates that the adsorption of TCIPP by biochar is mainly chemical, and the main speed control stage is the internal diffusion of particles. Isothermal adsorption shows that the adsorption process is mainly surface adsorption, and the total adsorption amount increases significantly with the increase of biochar temperature, from 0.8837 mg/g to 2.2574 mg/g. The adsorption mainly includes pore filling, hydrogen bonding, hydrophobic interaction, P-π interaction, and electrostatic attraction. As the temperature of biochar increases, the adsorption effect of biochar on TCIPP improves significantly, among which pore filling, P-π interaction, and hydrophobic interaction increase significantly, while hydrogen bonding decreases.

Data availability

Data is provided within the manuscript or supplementary information files.

Received: 2 July 2024; Accepted: 21 October 2024
Published online: 28 October 2024

References

1. Xu, G. et al. Recent advances in Biochar Applications in Agricultural soils: benefits and environmental implications. *Clean-Soil Air Water*. **40** (10), 1093–1098 (2012).
2. Sakhiya, A. K., Anand, A. & Kaushal, P. Production, activation, and applications of biochar in recent times. *Biochar*. **2** (3), 253–285 (2020).
3. Ravindiran, G. et al. Production and modifications of biochar to engineered materials and its application for environmental sustainability: a review. *Biochar*. **6**, 62 (2024).
4. Fernanda, R. et al. Environmental application of biochar: current status and perspectives. *Bioresour. Technol.* **246**, 110–122 (2017).
5. Sivaranjanee, R. et al. A critical review on biochar for the removal of toxic pollutants from water environment. *Chemosphere*. **360**, 142382 (2024).
6. Raj, A. et al. Preparation, characterization and agri applications of biochar produced by pyrolysis of sewage sludge at different temperatures. *Sci. Total Environ.* **795**, 148722 (2021).
7. Zhang, P. et al. Characteristics of tetracycline adsorption by cow manure biochar prepared at different pyrolysis temperatures. *Bioresour. Technol.* **285**, 121348 (2019).
8. Zhang, G. et al. Sorption of simazine to corn straw biochars prepared at different pyrolytic temperatures. *Environ. Pollut.* **159** (10), 2594–2601 (2011).
9. Chen, B. & Chen, Z. Sorption of naphthalene and 1-naphthol by biochars of orange peels with different pyrolytic temperatures. *Chemosphere*. **76** (1), 127–133 (2009).
10. Ni, N. et al. Biochar reduces the bioaccumulation of PAHs from soil to carrot (Daucus carota L.) in the rhizosphere: a mechanism study. *Sci. Total Environ.* **601–602**, 1015–1023 (2017).

11. Wang, Y. et al. Reducing the bioavailability of PCBs in soil to plant by biochars assessed with triolein-embedded cellulose acetate membrane technique. *Environ. Pollut.* **174**, 250–256 (2013).
12. Nazal, M. et al. Treatment of water contaminated with petroleum hydrocarbons using a biochar derived from seagrass biomass as low-cost adsorbent: isotherm, kinetics and reusability studies. *Sep. Sci. Technol.* **57**, 2358–2373 (2022).
13. Luo, Q. et al. Phytotoxicity of tris-(1-chloro-2-propyl) phosphate in soil and its uptake and accumulation by pakchoi (Brassica chinensis L. Cv. SuZhou). *Chemosphere*. **277**, 130347 (2021).
14. Luo, Q. et al. Distribution, source apportionment and ecological risks of organophosphate esters in surface sediments from the Liao River, Northeast China. *Chemosphere*. **250**, 126297 (2020).
15. Luo, Q. et al. Levels, distribution, and sources of organophosphate flame retardants and plasticizers in urban soils of Shenyang, China. *Environ. Sci. Pollut. Res.* **25** (31), 31752–31761 (2018).
16. Wang, Y. et al. A nationwide survey of 19 organophosphate esters in soils from China: spatial distribution and hazard assessment. *Sci. Total Environ.* **671**, 528–535 (2019).
17. Wang, R. et al. Occurrence and spatial distribution of organophosphate ester flame retardants and plasticizers in 40 rivers draining into the Bohai Sea, North China. *Environ. Pollut.* **198**, 172–178 (2015).
18. Lee, S. et al. Organophosphate flame retardants (OPFRs) in water and sediment: occurrence, distribution, and hotspots of contamination of Lake Shihwa, Korea. *Mar. Pollut. Bull.* **130**, 105–112 (2018).
19. Li, Y. J. et al. Adsorption characteristics and mechanisms of tris(2-chloroisopropyl)phosphate from corn straw biochar. *J. Agro-Environment Sci.* **42** (1), 112–120 (2023). (in Chinese).
20. Boehm, H. P. Some aspects of the surface chemistry of carbon blacks and other carbons. *Carbon*. **32** (5), 759–769 (1994).
21. Luo, Q. et al. Solvent demulsification-dispersive liquid-liquid microextraction based on solidification of floating organic drop coupled with ultra-high-performance liquid chromatography tandem mass spectrometry for simultaneous determination of 13 organophosphate esters in aqueous samples. *Sci. Rep.* **9**, 11292 (2019).
22. Yu, J. et al. Sorption characteristics and mechanism of oxytetracycline in water by modified biochar derived from chestnut shell. *China Environ. Sci.* **41** (12), 5688–5700 (2021). (in Chinese).
23. Wang, F. & Sun, H. W. Sorption mechanisms of polar and apolar organic contaminants onto biochars. *Environ. Chem.* **35** (6), 1134–1141 (2016). (in Chinese).
24. Chen, B. L., Zhou, D. D. & Zhu, L. Z. Transitional adsorption and partition of nonpolar and polar aromatic contaminants by biochars of pine needles with different pyrolytic temperatures. *Environ. Sci. Technol.* **42** (14), 5137–5143 (2008).
25. Hossain, M. K. et al. Influence of pyrolysis temperature on production and nutrient properties of wastewater sludge biochar. *J. Environ. Manage.* **92** (1), 223–228 (2011).
26. Yang, H. J. et al. Preparation of biochar from Solidago canadensis L. stalk and its pyridine adsorption performance. *Environ. Chem.* **40** (6), 1922–1932 (2021). (in Chinese).
27. Yao, Y. et al. Biochar derived from anaerobically digested sugar beet tailings: characterization and phosphate removal potential. *Bioresour. Technol.* **102** (10), 6273–6278 (2011).
28. Wang, Y. et al. Comparisons of biochar properties from wood material and crop residues at different temperatures and residence times. *Energy Fuels*. **27** (10), 5890–5899 (2013).
29. Zhao, Y. et al. Effect of pyrolysis temperature on char structure and chemical speciation of alkali and alkaline earth metallic species in biochar. *Fuel Process. Technol.* **141**, 54–60 (2016).
30. Fan, Q. et al. Effects of chemical oxidation on surface oxygen-containing functional groups and adsorption behavior of biochar. *Chemosphere*. **207**, 33–40 (2018).
31. Xu, Y. et al. Enhanced adsorption of methylene blue by citric acid modification of biochar derived from water hyacinth (Eichornia crassipes). *Environ. Sci. Pollut. Res.* **23** (23), 23606–23618 (2016).
32. Zheng, H. et al. Sorption of antibiotic sulfamethoxazole varies with biochars produced at different temperatures. *Environ. Pollut.* **181**, 60–67 (2013).
33. Chen, Y. C. et al. Preparation of Eucommia ulmoides lignin-based high-performance biochar containing sulfonic group: synergistic pyrolysis mechanism and tetracycline hydrochloride adsorption. *Bioresour. Technol.* **329**, 124856 (2021).
34. Hou, W. et al. Removal of malachite green dye from wastewater by different organic acid-modified natural adsorbent: kinetics, equilibriums, mechanisms, practical application, and disposal of dye-loaded adsorbent. *Environ. Sci. Pollut. Res.* **21** (19), 11552–11564 (2014).
35. Chen, T. et al. Sorption of tetracycline on H_3PO_4 modified biochar derived from rice straw and swine manure. *Bioresour. Technol.* **267**, 431–437 (2018).
36. Luo, J. W. et al. Sorption of norfloxacin, sulfamerazine and oxytetracycline by KOH-modified biochar under single and ternary systems. *Bioresour. Technol.* **263**, 385–392 (2018).
37. Dong, X., Ma, L. Q. & Li, Y. Characteristics and mechanisms of hexavalent chromium removal by biochar from sugar beet tailing. *J. Hazard. Mater.* **190** (1–3), 909–915 (2011).
38. Ahmad, M. et al. Trichloroethylene adsorption by pine needle biochars produced at various pyrolysis temperatures. *Bioresour. Technol.* **143**, 615–622 (2013).
39. Zhang, P. et al. Adsorption and catalytic hydrolysis of carbaryl and atrazine on pig manure-derived biochars: impact of structural properties of biochars. *J. Hazard. Mater.* **244–245**, 217–224 (2013).
40. Zhu, L. Z. & Chen, B. L. Sorption behavior of p-nitrophenol on the interface between anion-cation organobentonite and water. *Environ. Sci. Technol.* **34**, 2997–3002 (2000).
41. Bauzá, A. et al. Pnicogen-π complexes: theoretical study and biological implications. *Phys. Chem. Chem. Phys.* **14** (40), 14061–14066 (2012).
42. Liao, Q. et al. Strong adsorption properties and mechanism of action with regard to tetracycline adsorption of double-network polyvinyl alcohol-copper alginate gel beads. *J. Hazard. Mater.* **422**, 126863 (2022).

Author contributions

Qing Luo: Conceptualization, Writing, Supervision, Funding acquisition. Yongyao Deng: Investigation, Visualization. Yujie Li: Investigation, Formal analysis. Qing He: Investigation. Huiqiu Wu: Formal analysis. Xu Fang: Formal analysis.

Funding

This work was funded by the Applied Basic Research Program of Liaoning Province (No. 2023JH2/101300015), the Liaoning Revitalization Talents Program (No. XLYC2203141), and the Young and Middle-aged Scientific and Technological Innovation Talents Project of Shenyang (No. RC220128).

Declarations

Competing interests
The authors declare no competing interests.

Additional information
Supplementary Information The online version contains supplementary material available at https://doi.org/10.1038/s41598-024-77299-5.

Correspondence and requests for materials should be addressed to Q.L.

Reprints and permissions information is available at www.nature.com/reprints.

Publisher's note Springer Nature remains neutral with regard to jurisdictional claims in published maps and institutional affiliations.